

## Electronic Supplementary Information for

### Fabrication of Wide-detection-range H<sub>2</sub> Sensors with Controllable Saturation Behavior using Au@Pd Nanoparticle Arrays

Hui Yang,<sup>a</sup> Shuang Yang,<sup>a</sup> Qian Li,<sup>a</sup> Xuemin Zhang,<sup>\*a</sup> Tieqiang Wang,<sup>a</sup> Zhimin Gao,<sup>a</sup> Liying Zhang,<sup>a</sup> Lei Guo<sup>\*b</sup> and Yu Fu<sup>\*a</sup>

<sup>a</sup> Department of Chemistry, College of Sciences, Northeastern University, Shenyang 110819, P. R. China, E-mail: zhangxuemin@neu.edu.cn; fuyu@mail.neu.edu.cn.

<sup>b</sup> Texas A&M Institute of Biosciences & Technology, Houston, TX 77030, United States of America. E-mail: guoleijay@tamu.edu.

#### Experimental section

##### Materials.

Glass slides (15 × 30 mm<sup>2</sup>) used as substrates were cleaned by immersion in aqua regia solution (3:1, HCl:HNO<sub>3</sub>) followed by piranha solution (7:3 concentrated H<sub>2</sub>SO<sub>4</sub>/30% H<sub>2</sub>O<sub>2</sub>) and then rinsed repeatedly with Milli-Q water (18.2 MΩ cm). All chemical reagents were used as received without any purification.

##### Preparation of Au NPs.

Aqueous gold sol with average diameter of ~17 nm was prepared according to the method of Frens.<sup>[1]</sup> Briefly, 1.21 mL of 1% aqueous HAuCl<sub>4</sub>·3H<sub>2</sub>O solution was added to 100 mL of triply deionized water, which was then boiled. After that 4 mL of 1% sodium citrate was added to the solution, which was then boiled for 20 min, obtaining gold nanoparticle of ~17 nm with an absorption band located at 520 nm.

##### Preparation of Au@Pd NPs.

Au@Pd NPs were synthesized by a seed-growth method.<sup>[2]</sup> In brief, 223 μL of H<sub>2</sub>PdCl<sub>4</sub> (52.4 mM) was mixed into 30 mL Au sol. After that, a mixture of 1.27 mL of sodium citrate (1%), 2.54 mL L-ascorbic acid (1%) and 5.89 mL water was added dropwisely into the

system with continuous stirring for 1h. The obtained Pd shell is ~2 nm. If the amount of H<sub>2</sub>PdCl<sub>4</sub> was changed into 380 μL and 829 μL, the obtained Pd shell thickness are 4 nm and 6 nm, respectively.

### **Preparation of Pd NPs.**

520 μL of H<sub>2</sub>PdCl<sub>4</sub> (52.4 mM) was added to 100mL of water. After that a mixture of 4 mL of sodium citrate (1%) and 4 mL L-ascorbic acid (1%) was added to the solution dropwisely, which was then stirred for ~1 h.

### **Preparation of Au@Pd NAs.**

Au@Pd NAs on glass substrate were prepared by lifting up of gold monolayer from water/hexane interface as described previously.<sup>[3,4]</sup> Briefly, 10 mL of aqueous Au@Pd sol was added to a weighting bottle (inner dimension, 3 × 3 × 6 cm<sup>3</sup>), and 2 mL of hexane was added to the top of the colloid solution surface to form an immiscible water/hexane interface. About 4 mL of absolute ethanol was then added dropwisely to the hexane layer, which led to Au@Pd NPs trapped at the interface. After the hexane layer was evaporated, the Au@Pd NAs were transferred to glass substrate using the lift-up method. In addition to glass substrate, Au@Pd NAs could also be transferred to TEM copper grid for measurement.

### **Preparation and characterization of sensing performance of sensors.**

Conductive silver paste was dropped on the surface of Au@Pd NAs with separation of ~0.5 cm, and then dried in air. The H<sub>2</sub> sensing performance of as-prepared samples were evaluated using a gas sensing analysis system (CGS-MT, Beijing Elite Tech Co) equipped with a dynamic gas distribution system at 25 °C. Air was used as carrier gas. 1 V voltage was applied between electrodes. Before sensing performance testing, all the freshly prepared sensors were preconditioned in cyclic H<sub>2</sub> and air atmosphere for several hours until they achieved a stable baseline. The sensor response is defined as  $(I_g - I_a)/I_a$ , where  $I_g$  and  $I_a$  are the electrical current of sensor in H<sub>2</sub> and air, respectively.

## Characterization.

The morphology of the Au@Pd NAs were examined using a Hitachi SU1080 field emission scanning electron microscope operating at primary electron energy of 15 kV. TEM images were conducted using a JEOL 2100F electron microscope operating at primary electron energy of 200 kV.

**Table S1.** A summary of the saturation behavior of previously reported wide-detection-range H<sub>2</sub> sensors

Morphology	Detection Range	FOM <sub>10</sub> <sup>*a</sup>	FOM <sub>50</sub> <sup>*a</sup>	Ref.
Pd/Ag Mesowire	0.1-100%	~0.50	~0.20	5
Pd/Cr Nanowire	0.1-100%	~0.40	~0.10	6
Pd/Au@PETF	5 ppm-100%	~0.43	~0.14	7
Pd Nanodots	0.1-100%	~0.73	~0.10	8
Pd NAs	0.05-100%	~0.05	~0.03	9
Pd/Ni NAs	0.05-100%	~0.05	N.A. <sup>b</sup>	9
Au@Pd (17/2) NAs	0.1-100%	~0.38	~0.10	This Work
Au@Pd (17/4) NAs	0.1-100%	~0.83	~0.48	This Work

<sup>a</sup> All these data are estimated from figures given in corresponding references. For a sensor with response increasing lineally with H<sub>2</sub> concentration, FOM<sub>10</sub><sup>\*</sup>=0.9 and FOM<sub>50</sub><sup>\*</sup>=0.5. <sup>b</sup> N.A.=not mentioned

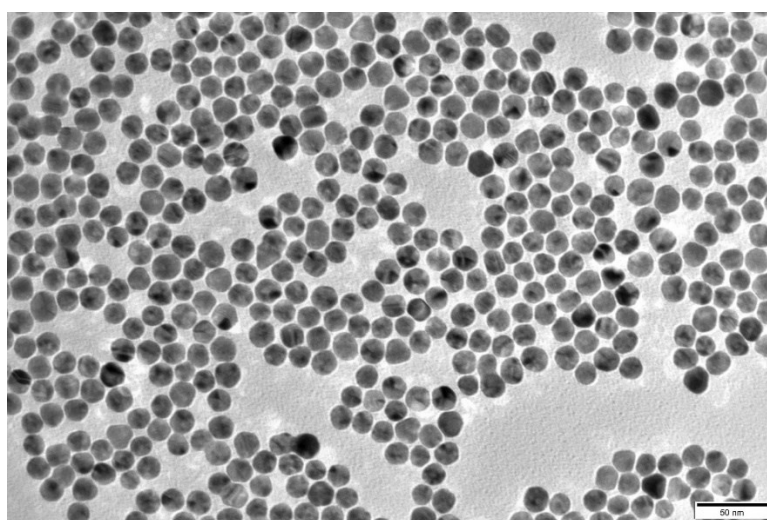


**Fig. S1** TEM image of Au NAs, and the diameter of Au nanoparticle is ~17 nm.

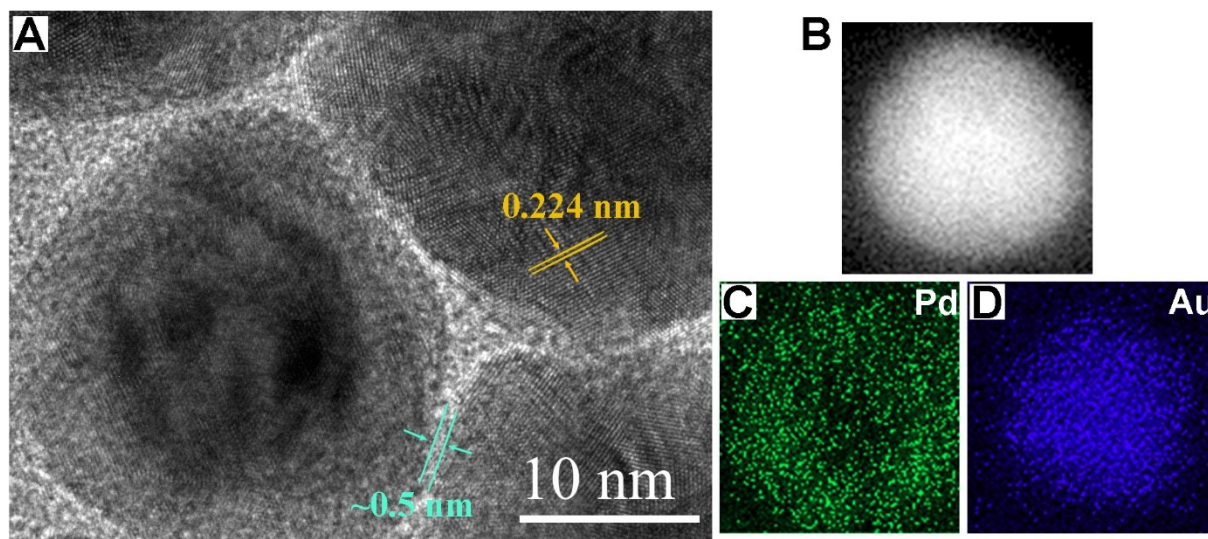


**Fig. S2** High-resolution TEM image of Au@Pd NAs (A). The interplanar spacing between the adjacent lattice fringes in the shell area is 0.224 nm, which corresponds to the (111) plane of Pd. The interparticle distances is  $\sim 0.5$  nm. STEM image (B) and corresponding EDX elemental mappings (C, D) of a single Au@Pd nanoparticle.

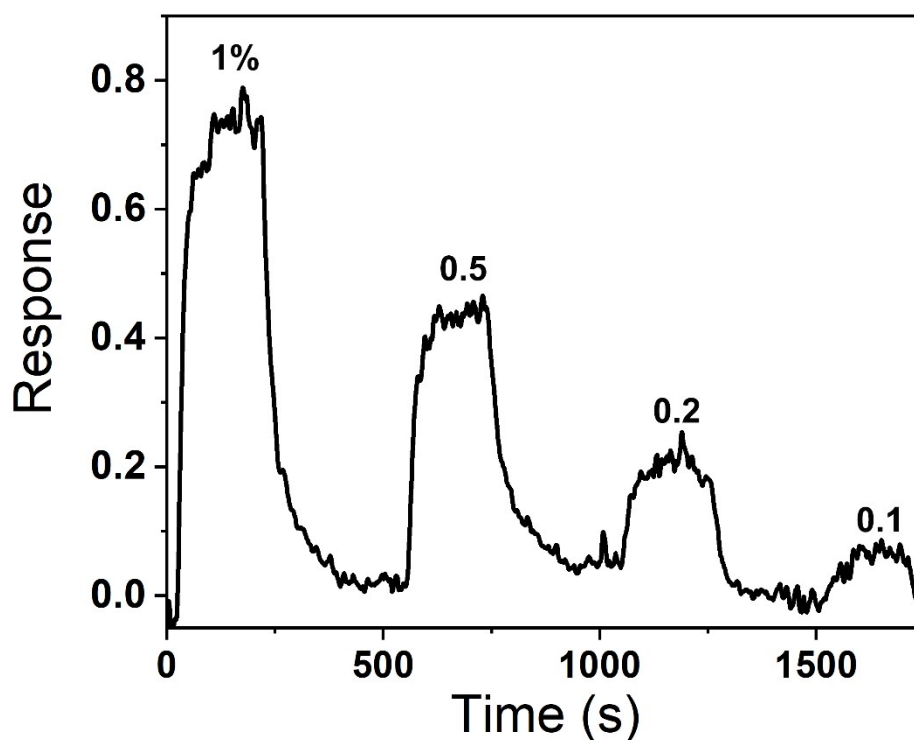


**Fig. S3** Response of Au@Pd (17/2) NAs to 1-0.1% H<sub>2</sub>.

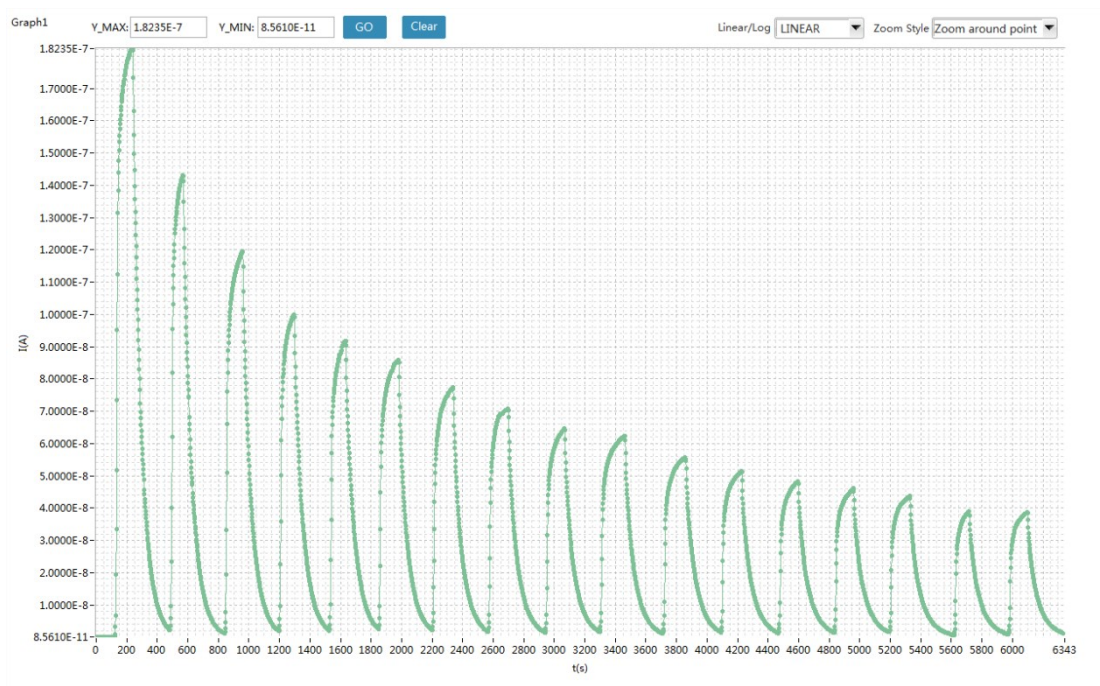


**Fig. S4** Real-time current variation of Au@Pd (17/4) NAs to 50% H<sub>2</sub> during preconditioning. It can be seen the response of the sensor decreases gradually due to the rearrangement of Au@Pd NPs.

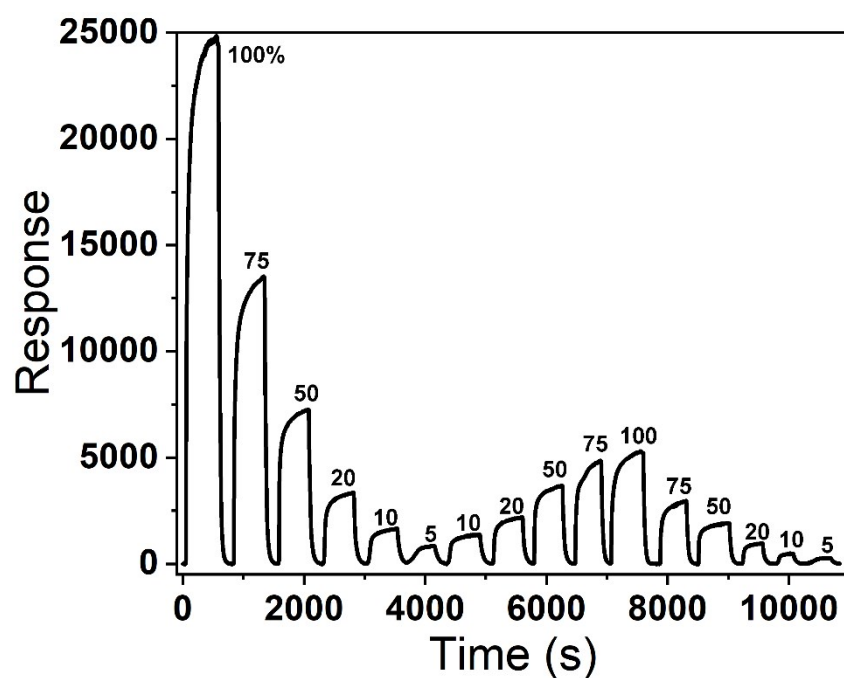


**Fig. S5** Response of Au@Pd (17/4) NAs to H<sub>2</sub> gas of various concentrations during preconditioning. During the preconditioning, Au@Pd (17/4) NAs are not able to detect H<sub>2</sub> gas reliably due to the rearrangement of NPs.

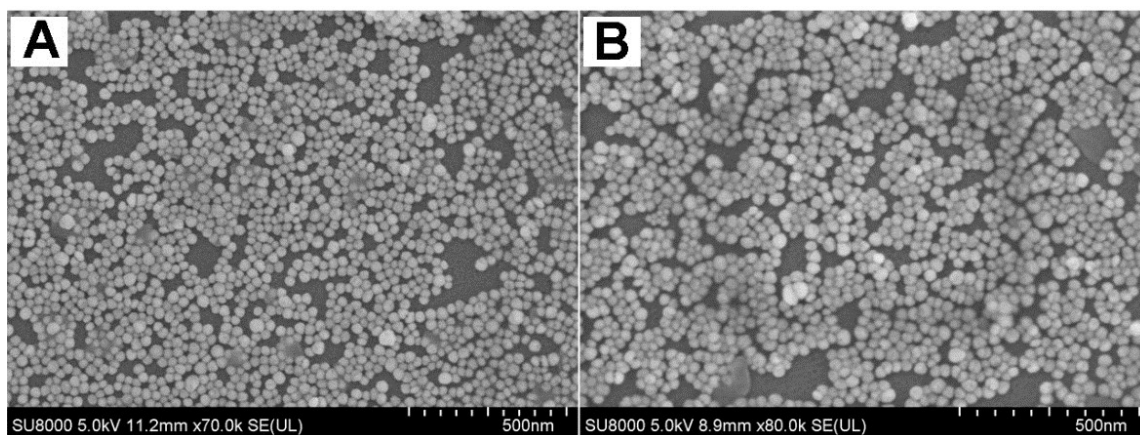


**Fig. S6** SEM images of Au@Pd (17/6) NAs before (A) and after (B) preconditioning. Cracks can be observed after the preconditioning

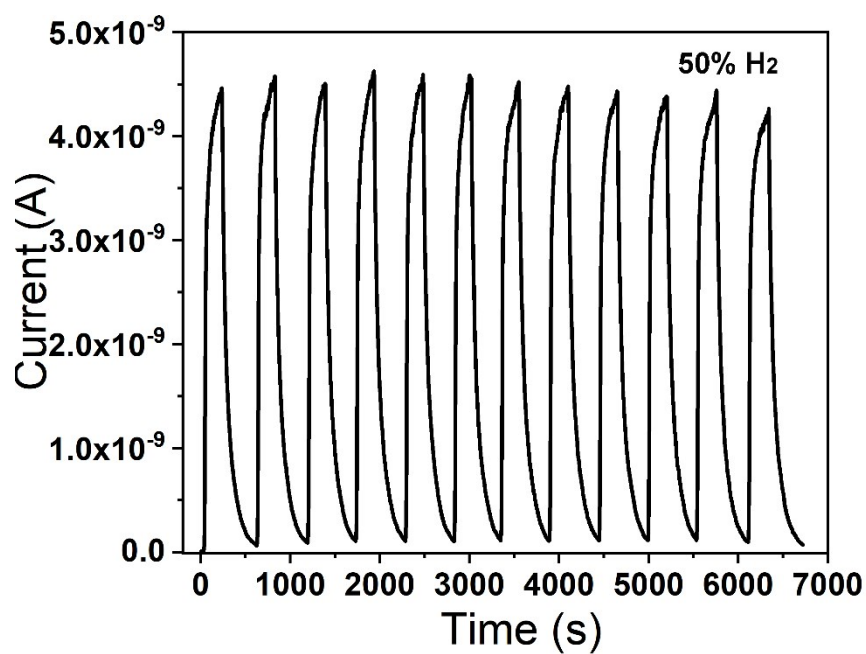


**Fig. S7** Cyclic current responses of Au@Pd (17/4) NPs to 50% H<sub>2</sub> after preconditioning.

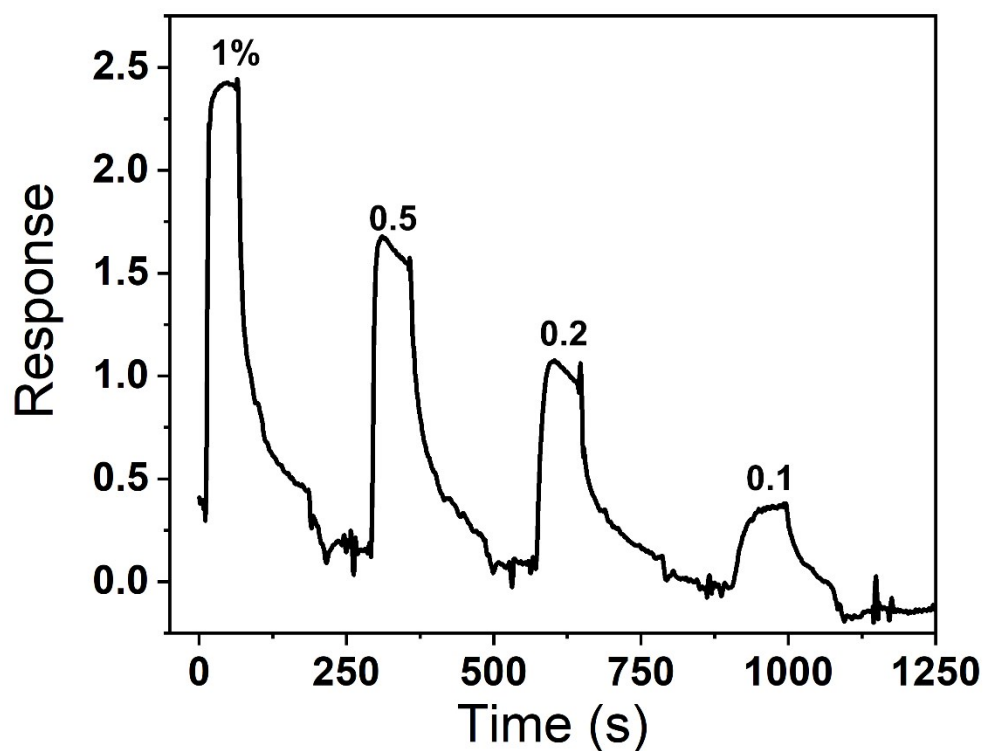


**Fig. S8** Response of Au@Pd (17/4) NAs to 1-0.1% H<sub>2</sub>.

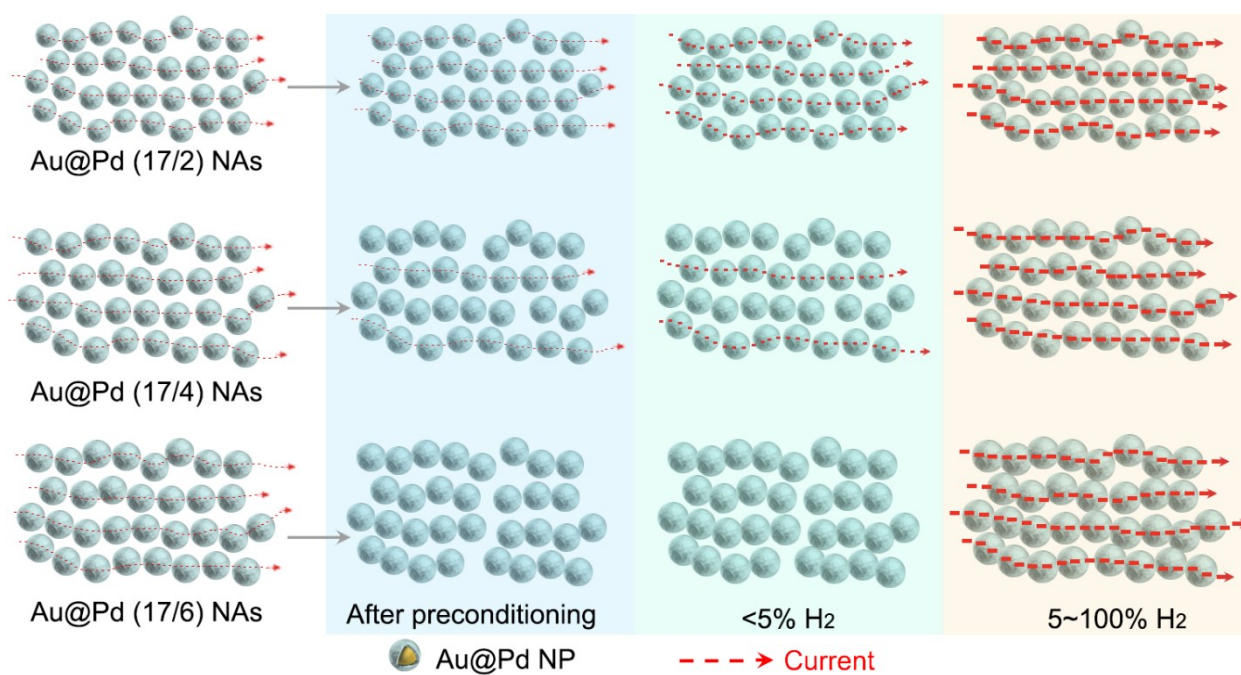


**Fig. S9** A schematic illustration for the possible sensing mechanism of Au@Pd NAs to H<sub>2</sub>.

### **A possible sensing mechanism for the detection of H<sub>2</sub> using Au@Pd NAs.**

A schematic illustration for the possible sensing mechanism of Au@Pd NAs to H<sub>2</sub> is given as **Fig. S9**.

For Au@Pd (17/2) NAs, the arrangement of NPs in NAs doesn't change after the preconditioning. When the sensor is exposed to H<sub>2</sub>, the lattice expansion of Pd shell reduces the mean gap size between NPs, which therefore promotes the electron hopping across the NAs. The presence of Au core suppresses the phase transition of Pd shell and makes the Pd lattice expansion gradually with the increase of H<sub>2</sub> concentration, leading to a wide detection range of 0.1~100%.

For Au@Pd (17/4) NAs, there is a moderate rearrangement of NPs after the preconditioning. Part of the Au@Pd NPs rearrange into NP segments with gaps of various sizes. This process reduces the number of current paths for electron hopping, which thus decreases the base current of the sensor. When sensors are exposed to H<sub>2</sub> with concentration less than 5%, only the electron hopping through the left current paths can be promoted, whereas the newly-generated gaps between NP segments can not be effectively reduced. As such, the sensing mechanism of Au@Pd (17/4) NAs to low-concentration H<sub>2</sub> (0.1~5%) are similar as Au@Pd (17/2) NAs. In contrast, when Au@Pd (17/4) NAs are exposed to high-concentration H<sub>2</sub> (>5%), not only the electron hopping through the existing current paths can be promoted, but also new current paths are able to be generated. Therefore, compared with Au@Pd (17/2) NAs, Au@Pd (17/4) NAs show a much more suppressed sensor saturation (and thus much higher FOM\*) at high-concentration H<sub>2</sub>.

With respect to Au@Pd (17/6) NAs, NPs show the most remarkable rearrangement. The left current paths after preconditioning are very rare (with base current of  $8 \times 10^{-13}$  A), thus the sensor shows almost no response to H<sub>2</sub> with concentration less than 5%. When exposed to high-concentration H<sub>2</sub>, Au@Pd (17/6) NAs have a similar behavior as Au@Pd (17/4) NAs.

As such, Au@Pd (17/6) NAs have high FOM\* between 5~100% H<sub>2</sub>, but lose their sensing ability to low-concentration H<sub>2</sub>.

## References

1. G. Frens, *Nature Phys. Sci.*, 1973, **241**, 20-22.
2. P. Fang, J. Li, Z. Yang, L. Li, B. Rin, Z. Tian, *J. Raman Spectrosc.*, 2018, **39**, 1679-1687.
3. F. Reincke, S. G. Hickey, W. K. Kegel, D. Vanmaekelbergh, *Angew. Chem. Int. Ed.*, 2004, **43**, 458-462.
4. X. Zhang, J. Zhang, H. Wang, Y. Hao, X. Zhang, T. Wang, Y. Wang, R. Zhao, H. Zhang, B. Yang, *Nanotechnology*, 2010, **21**, 465702.
5. C. Fournier, K. Rajoua, M. L. Doublet, F. Favier, *ACS Appl. Mater. Interfaces*, 2013, **5**, 310-318.
6. X. Zeng, Y. Wang, H. Deng, M. L. Latimer, Z. L. Xiao, J. Pearson, T. Xu, H. Wang, U. Welp, G. W. Crabtree, W. K. Kwok, *ACS Nano*, 2011, **5**, 7443–7452.
7. F. A. A. Nugroho, I. Darmadi, L. Cusinato, A. Susarrey-Arce, H. Schreuders, L. J. Bannenberg, A. B. da Silva Fanta, S. Kadkhodazadeh, J. B. Wagner, T. J. Antosiewicz, A. Hellman, V. P. Zhdanov, B. Dam, C. Langhammer, *Nat. Mater.*, 2019, **18**, 489-495.
8. L.G. Villanueva, F. Fargier, T. Kiefer, M. Ramonda, J. Brugger, F. Favier, *Nanoscale*, 2012, **4**, 1964-1967.
9. L. Sun, M. Chen, X. Peng, B. Xie, M. Han, *Int. J. Hydrog. Energy.*, 2016, **41**, 1341-1347.